🄳 Jyoti Biswas, 🄳 Erdong Wang, 🄳 Mengjia Gaowei, et al.

**COLLECTIONS**

🄵 This paper was selected as Featured

🄴🄿 This paper was selected as an Editor's Pick

🅂🄲🄸 This paper was selected as Scilight

View Online    Export Citation    CrossMark

---

**ARTICLES YOU MAY BE INTERESTED IN**

Revisiting heat treatment and surface activation of GaAs photocathodes: In situ studies using scanning tunneling microscopy and photoelectron spectroscopy
Journal of Applied Physics **128**, 045308 (2020); https://doi.org/10.1063/5.0008969

Improved lifetime of a high spin polarization superlattice photocathode
Journal of Applied Physics **127**, 124901 (2020); https://doi.org/10.1063/1.5139674

Rugged spin-polarized electron sources based on negative electron affinity GaAs photocathode with robust $Cs_2Te$ coating
Applied Physics Letters **112**, 154101 (2018); https://doi.org/10.1063/1.5026701

## AIP Advances
## Mathematical Physics Collection

READ NOW

---
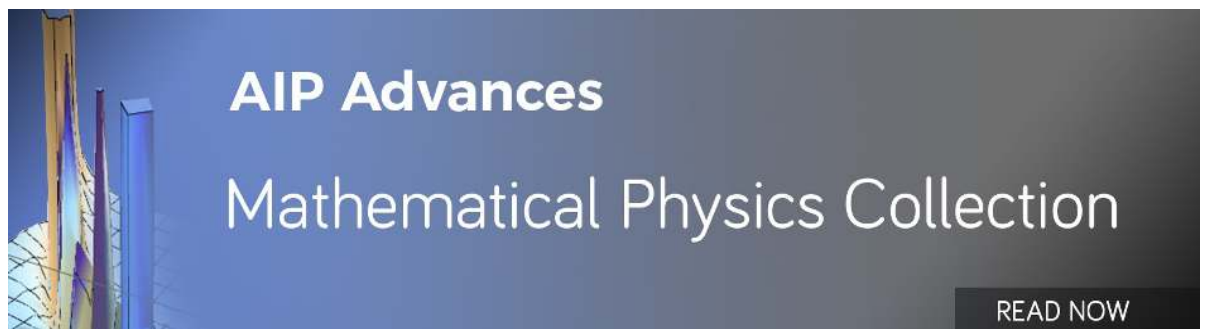
# High quantum efficiency GaAs photocathodes activated with Cs, O$_2$, and Te  (F) (SCI) (EP)

View Online     Export Citation     CrossMark

Jyoti Biswas,[1] (iD) Erdong Wang,[2,a] (iD) Mengjia Gaowei,[2] (iD) Wei Liu,[2] Omer Rahman,[2] and Jerzy T. Sadowski[3] (iD)

### AFFILIATIONS

[1] Department of Physics and Astronomy, Stony Brook University, Stony Brook, New York 11794, USA
[2] Collider Accelerator Department, Brookhaven National Laboratory, Upton, New York 11973, USA
[3] Center for Functional Nanomaterials, Brookhaven National Laboratory, Upton, New York 11973, USA

[a] Author to whom correspondence should be addressed: wange@bnl.gov

### ABSTRACT

GaAs photocathodes are the primary choice for generating spin-polarized electron beam with high brightness, high polarization, and fast polarization reversal. However, it suffers from short lifetime due to the highly reactive nature of the emission surface, resulting in substantial operational difficulties. Activating GaAs with a more robust material, such as Cs$_2$Te, shows comparable polarization to that of Cs–O activation and increases the lifetime due to the robustness of the Cs$_2$Te layer. However, previously reported photocathodes based on Cs–Te activation on GaAs suffer from 10× lower quantum efficiency (QE) compared to that activated with conventional Cs–O activation. Herein, we report activation recipes for GaAs photocathodes using Cs, O$_2$, and Te. For Cs–Te activation, the QE was 6.6% at 532 nm. For Cs–O–Te activation, the QE was 8.8% at 532 nm and 4.5% at 780 nm. The negative electron affinity of the activated GaAs was directly measured and confirmed by low energy electron microscopy. We also report the activation layer chemical states and stoichiometry using *in situ* micro-spot synchrotron radiation x-ray photoelectron spectroscopy.

GaAs photocathode based polarized electron sources are the primary choice for accelerator facilities,[1–3] polarized electron microscopes,[4] and positron sources[5,6] around the world. A *p*-type GaAs sample coated with a small amount of Cs shows excellent photoemission properties, a phenomenon first reported in 1965.[7] Substantial research and developments have taken place since then to improve the quantum efficiency (QE), lifetime, spin polarization, and other parameters of such sources. GaAs coated with Cs and an oxidant (oxygen or NF$_3$) has been found to form a negative electron affinity (NEA) surface, which is necessary for polarized electron photoemission.[8–11] Illuminating the photocathode with circularly polarized light with energy just above the bandgap of GaAs leads to the photoemission of a spin-polarized electron beam. The typical spin polarization of strained-superlattice (SL) GaAs is 90% with a typical QE of around 1%, for a certain laser wavelength.[12–14] SL-GaAs with a distributed Bragg reflector has shown to increase the QE up to 6.4% with a spin polarization of 84%.[15]

The lifetime of GaAs photocathodes is limited due to a very sensitive Cs-oxidant layer.[16–18] The two main processes that cause the degradation of QE are vacuum poisoning[18,19] and ion back-bombardment[20,21] during beam operation. Due to the highly reactive Cs–O activation layer, the GaAs photocathode requires an extremely high vacuum environment to minimize the reaction of residual gas species with the activation layer and to operate reliably for a long time. To obtain a long lifetime, several laboratories are developing GaAs activation methods using a low electron affinity material, such as Cs$_2$Te and Cs$_3$Sb.[22–26] It has been shown that spin-polarized electrons can be extracted from the GaAs photocathode activated with Cs$_2$Te[22] or Cs$_3$Sb.[26] Cs$_3$Sb has a bandgap of about 1.6 eV, which is very close to the bandgap of GaAs (~1.42 eV). Thus, the layer of Cs$_3$Sb plays a detrimental effect on spin-polarized electron extraction from GaAs. Cs$_2$Te has a bandgap of 3.3 eV, and hence, illumination with ~780 nm light on Cs$_2$Te coated GaAs ensures photoemission from the GaAs only. A previous experiment showed that a Cs$_2$Te coated GaAs photocathode exhibited an improved lifetime, but a low QE (1.5% at 532 nm),[22] rendering the source ineffective for high current (>1 mA) applications.

In this study, we report a high quantum efficiency bulk GaAs photocathode activated with Cs, $O_2$, and Te. Our results show that an activation of the GaAs photocathode after high-temperature heat cleaning (590 °C–600 °C) is more efficient in reducing the native oxides from GaAs and improves the QE compared to the previously reported activation of a GaAs photocathode after low-temperature heat cleaning (~400 °C).[22] Here, we present activation recipes that form a better $Cs_2Te$ NEA state on GaAs, which in turn provides a much superior QE compared to other previously reported protocols. We characterized the photocathode using micro-spot synchrotron radiation x-ray photoelectron spectroscopy (XPS), low-energy electron microscopy (LEEM), and micro-spot low-energy electron diffraction (LEED).

Experiments were carried out at the x-ray photoemission electron microscopy (XPEEM) end-station of the Electron Spectro-Microscopy beamline (ESM, 21-ID-2) of the National Synchrotron Light Source II, Brookhaven National Laboratory (NSLS II, BNL). The end-station offers the possibility to perform LEEM, LEED, and XPEEM measurements at photon energies from 20 eV up to 1500 eV and has an integrated activation chamber. The base pressures in the photocathode activation chamber and the LEED/LEEM characterization chamber were around $1 \times 10^{-10}$ Torr and $3 \times 10^{-10}$ Torr, respectively. The two samples used in the measurements were Zn-doped p-type GaAs (100) wafers with a carrier concentration of $1 \times 10^{19}$ $cm^{-3}$, purchased from AXT, Inc. The sample preparation followed the recipe published elsewhere.[27]

To remove the native oxides and carbon contamination, the GaAs sample was heat-treated in the characterization chamber while monitoring the LEED pattern. The temperature of the sample was ramped at a rate of around 15 °C per min until a clear ($1 \times 1$) Ga rich surface reconstruction was observed in the LEED pattern. Figure 1(a) shows a micro-spot LEED pattern of GaAs taken after the desorption of oxides from the sample surface. The four sharp diffraction spots are ($1 \times 1$) spots from the GaAs (100) surface. The very weak additional spots in the background hint at a possible ($4 \times 6$) reconstruction, which would indicate that the sample was at 590 °C–600 °C.[28,29] There is also a significant diffused background, suggesting that the surface is rather disordered. During the heat treatment, the maximum pressure recorded was ~$1 \times 10^{-8}$ Torr in the LEED/LEEM chamber. After one hour of heat treatment, the sample was cooled down to room temperature. The sample was initially cooled down in the LEED/LEEM chamber, and once the temperature fell below 500 °C, it was transferred to the activation chamber to avoid slow cooling in the LEED/LEEM chamber. In the activation chamber, both activation and XPS could be performed. Once the sample temperature reached around room temperature, the pressure in the activation chamber was ~$2 \times 10^{-10}$ Torr. XPS was performed subsequently to check the cleanliness of the heat-cleaned sample. Figures 1(b) and 1(c) show that both gallium and arsenic oxide, which were prevalent in the air-exposed sample,[27] desorbed completely. The photon energies for acquiring the spectra of the As 3d and Ga 3d core levels were 140 eV and 120 eV, respectively. The energy resolution of the photoelectron detector was around 0.15 eV. Shirley background was subtracted from all the spectra, and peak fitting was performed using CasaXPS[30] with Lorentzian asymmetric line shape convoluted with a Gaussian. The binding energy of all the spectra was referenced to the C–C component of the C 1s peak of adventitious hydrocarbon at 285 eV.

The heat-cleaned GaAs (sample No. 1), once cooled down to room temperature, was activated by depositing Cs and Te using the traditional "yo-yo" technique[11,31,32]—a method commonly employed for Cs–O activation on GaAs. The Cs source was a commercial alkali metal dispenser (AMD) from SAES Getters.[33] For the Te source, we emptied an AMD, then ultrasonically cleaned it, and filled it up with ultra-high purity Te (99.9999%) powder. The evaporation rate of the Te source was calibrated using a quartz crystal monitor (QCM)[24] in a separate chamber, and it was 0.05 Å/s–0.07 Å/s during activation. We over-cesiated the surface until the photocurrent passed the peak value and dropped 30% from the peak value. The same steps were carried out for the Te deposition as well. The Cs and Te deposition cycles were performed repeatedly to obtain a photocurrent plateau. Figure 2(a) represents the activation curve of the Cs–Te activated photocathode. During the Cs–Te activation, the photocathode was illuminated with a 532 nm laser diode, and the photocurrent was measured with a Keithley picoammeter. The maximum QE observed at 532 nm illumination was 6.6%. Although this is the highest QE reported so far for Cs–Te activated GaAs photocathodes, it is still not as high as the QE of typical Cs–O activated GaAs photocathodes, typically ~10%.

To increase the QE and also to benefit from the robust $Cs_2Te$ layer, we performed activation using Cs, $O_2$, and Te on another heat-cleaned GaAs (sample No. 2). The oxygen will generate extra surface
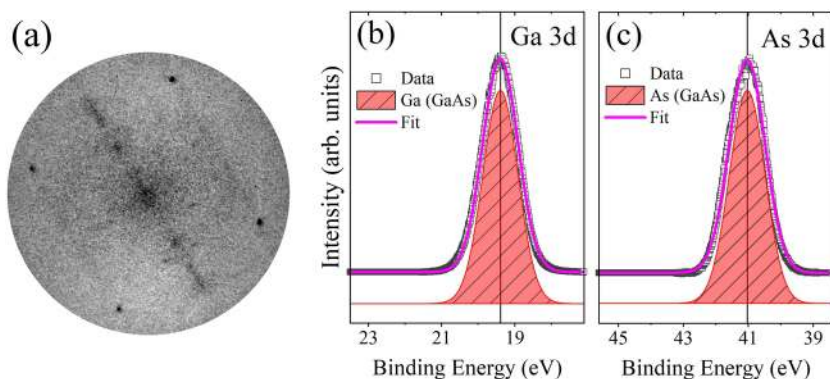


**FIG. 1**. (a) Micro-spot LEED pattern of the GaAs surface at 30 eV electron energy after the heat cleaning to remove the native oxide layer. During oxide desorption, the temperature of the sample was 590 °C–600 °C. Micro-spot synchrotron XPS spectra of (b) Ga 3d and (c) As 3d core levels after the sample was cooled down to room temperature. Shirley background is subtracted from the spectra. Data and corresponding fit are moved upward for clarity.
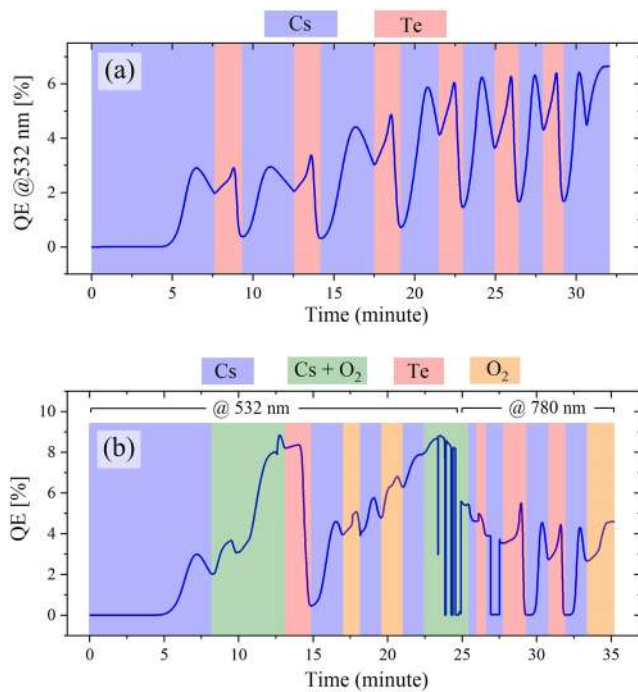
**FIG. 2.** (a) GaAs photocathode activation (sample No. 1) with alternate deposition of Cs and Te. The photocurrent was measured over time with 532 nm laser illumination, and the maximum QE in the measurement was 6.6%. (b) GaAs photocathode activation (sample No. 2) with Cs, O₂, and Te. The photocurrent was first measured with 532 nm laser illumination, and once photocurrent reached the plateau (at ∼25 min), the illumination was switched to 780 nm to check the QE in the infrared region. The maximum QE at 532 illumination was 8.8% and 4.5% at 780 nm illumination, respectively.

dipole with Cs, which will in principle reduce the electron affinity further.[32] We have previously confirmed that this type of activation involving Cs, O₂, and Te yields a charge lifetime around 5–6 times more than that in traditional Cs–O based GaAs photocathodes.[24] Charge lifetime is the amount of charge that can be extracted until the photocathode QE drops to $1/e$ of its initial value and is an important parameter for comparing the performance of different photocathodes. In this case, as a first step, we achieved a photocurrent peak using Cs and then obtained a photocurrent plateau by co-deposition of Cs and O₂. A 532 nm laser diode was used to measure the QE during activation. Once the photocurrent reached the plateau via the co-deposition of Cs and O₂, initially Te deposition was performed. The Te deposition rate was 0.05 Å/s–0.07 Å/s, same as that in the case of Cs–Te activation. Based on the QCM calibration,[24] the thickness of the Te layer was 0.7 ± 0.1 nm. The deposition of Te onto the Cs–O activated layer caused a rapid decrease of QE, and then, we maximized the QE by alternate Cs and O₂ deposition until the maximum QE was reached. At this stage (∼25 min of activation), we switched to 780 nm laser illumination to check the QE. Subsequent deposition of Cs and Te did not improve the QE further. Thus, we conclude that the Cs–O–Te activation is completed after maximizing the QE at around 25 min. Details of the activation process are shown in Fig. 2(b). This activation technique provides

a higher photocurrent, both for the visible and infrared regions. The maximum QE we obtained was 8.8% at 532 nm and 4.5% at 780 nm.

After activation, the photocathode was moved into the LEED/LEEM characterization chamber to measure the decrease in the work function of the activated GaAs photocathode. The work function is the energy difference between the vacuum level and Fermi energy ($E_F$). In the LEEM setup, 20 keV electrons leaving from the objective lens are decelerated by the sample bias of $-20 + V_o$ kV, where $V_o$ is the so-called start voltage. By increasing the start voltage $V_o$, one can slowly switch from the mirror mode, where all electrons are reflected, to the LEEM mode, where all electrons interact with the sample.[34,35] The intensities of the reflected/back-scattered electrons vs start voltage (LEEM I/V) in Cs–Te activated (sample No. 1) and in Cs–O–Te activated (sample No. 2) are shown in Figs. 3(a) and 3(b), respectively. The blue curve was obtained from a heat-cleaned sample before activation, and the red curve was obtained from the same sample after the activation. The decrease in work function after Cs–Te activation was 2.8 eV, and after Cs–O–Te activation, it was 3.2 eV.

The work function of the activated photocathode ($\Phi_f$) equals the initial work function before the activation ($\Phi_i$) minus the change in work function after the activation (e.g., $\Phi_f = \Phi_i - \Delta\Phi$). We measured the work function of the heat-cleaned sample before activation as 4.2 eV. Based on the work function reduction described in Figs. 3(a) and 3(b), the final work function $\Phi_f$ was 1.4 eV after Cs–Te activation and 1.0 eV after Cs–O–Te activation. In a heavily p-doped semiconductor, the condition for effective NEA is that the final work function needs to be lower than the bandgap of the semiconductor ($\Phi_f < E_g$).[36] As shown in Fig. 3(c), for both Cs–Te and Cs–O–Te activation, the final work function is lower than the bandgap of GaAs, satisfying the condition for an effective NEA ($\chi_{eff} < 0$). The value of $\chi_{eff}$ equals ($\Phi_f - E_g$), assuming $\Phi_f < E_g$. In the Cs–Te activation, the effective electron affinity $\chi_{eff}$ is $-0.02$ eV, whereas in Cs–O–Te activation the effective electron affinity $\chi_{eff}$ is $-0.42$ eV. The effective NEA we found here is slightly higher than previously reported values.[23,37] For example, Sugiyama *et al.* reported an effective NEA of $-0.1$ eV for Cs–Te activation,[23] and Zhang *et al.* reported an effective NEA of $-0.5$ eV for traditional Cs–O activation.[37] Jin *et al.* measured a 3.5 eV work function reduction in Cs–O activation.[11] It should be noted that the effective NEA is dependent on the work function reduction. During our LEEM I/V measurement, the vacuum pressure in the LEED/LEEM characterization chamber increased to around $5 \times 10^{-9}$ Torr, which resulted in a gradual increase of the work function. It is estimated that during the LEEM I/V measurement of the Cs–O–Te activated cathode, the work function increased by around 0.3 eV–0.4 eV due to the pressure increase in the chamber. Thus, we state that the value of the effective NEA $\chi_{eff}$ we presented here is the up-limit; the initial value of $\chi_{eff}$ was even lower than that.

We performed micro-spot synchrotron radiation x-ray photoelectron spectroscopy on Cs–Te and Cs–O–Te activated photocathodes. The photon energies used for acquiring the Cs $3d_{5/2}$, Te $3d_{5/2}$, O 1s, C 1s, As 3d, and Ga 3d core level spectra were 833 eV, 673 eV, 633 eV, 383 eV, 140 eV, and 120 eV, respectively. The photon energy was varied to maintain the kinetic energy of photoelectrons at around 100 eV, which resulted in a small inelastic mean free path (IMFP); thus, measurements were very surface sensitive.
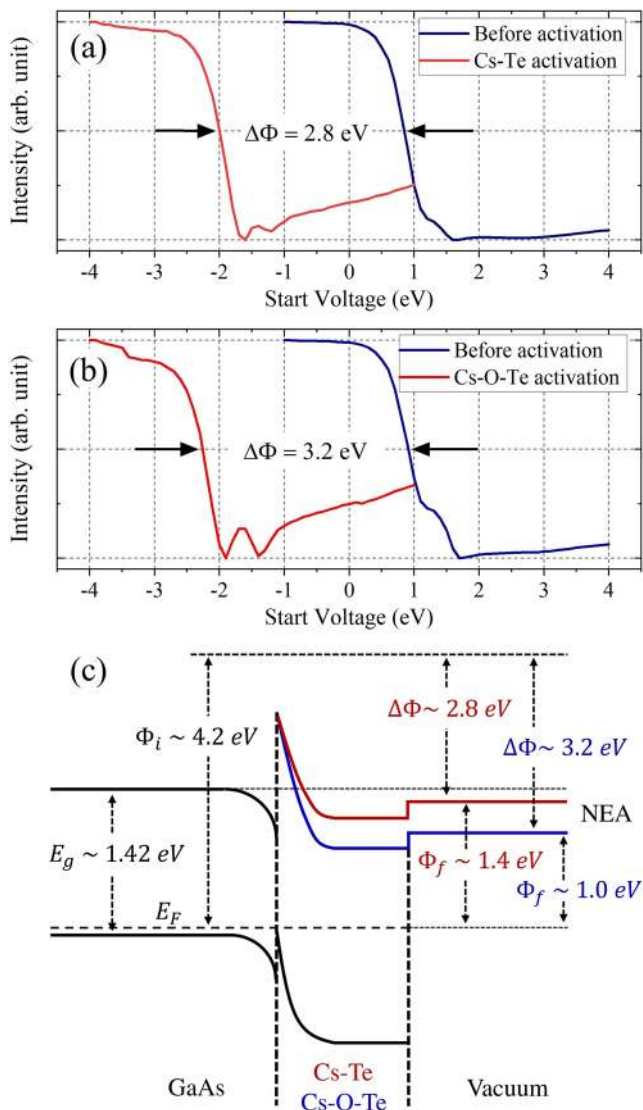
**FIG. 3.** (a) LEEM I/V measurement of GaAs (sample No. 1) after heat cleaning but before activation (blue line), and after Cs–Te activation (red line). The decrease in the work function was 2.8 eV. (b) LEEM I/V measurement of GaAs (sample No. 2) after heat cleaning but before the activation (blue line), and after Cs–O–Te activation (red line), respectively. The decrease in the work function was 3.2 eV. (c) Sketch of the energy band diagram of GaAs with Cs–Te/Cs–O–Te activation layer deduced from the LEEM I/V measurements. Both in Cs–Te and Cs–O–Te activation, the vacuum level lies below the conduction band minimum in the bulk of GaAs, thus creating the NEA surface.

Figure 4 shows the micro-spot synchrotron XPS spectra of the Cs $3d_{5/2}$, Te $3d_{5/2}$, Ga $3d$, and As $3d$ core levels after the photocathode activation with Cs and Te, as described in Fig. 2(a). The Te $3d_{5/2}$ spectrum shown in Fig. 4(b) consists of both the Cs$_2$Te compound (~571.5 eV) and covalent Te (~572.9 eV). The peak positions of Cs$_2$Te and covalent Te were identified from previously published data.[38,39]

Figure 5 shows the micro-spot synchrotron XPS spectra of the Cs $3d_{5/2}$, Te $3d_{5/2}$, O $1s$, Ga $3d$, and As $3d$ core levels after the photocathode activation with Cs, O$_2$, and Te, as described in Fig. 2(b). This activation was preceded by the usual activation using Cs–O, then deposition of the Cs–Te layer, and finally, the improvement of the QE by alternate deposition of Cs and O$_2$. The Te $3d_{5/2}$ spectrum in Fig. 5(b) shows the formation of both Cs$_2$Te and covalent Te. The oxygen spectrum in Fig. 5(c) has a contribution from surface dipoles, such as GaAs–O–Cs and the interface layer, which consists of Ga oxide [Fig. 5(d)] and As oxide [Fig. 5(e)]. Once native oxides were desorbed from the GaAs surface by thermal cleaning, the surface became sensitive to oxygen; it has been previously observed that the oxygen exposure during activation could contribute to the formation of GaAs oxides.[40] Since the synchrotron XPS measurement was very surface-sensitive, the oxide peaks that appeared in the XPS spectra after activation correspond to a minuscule amount of oxide on the surface.

In Table I, we show the ratios between Cs, O$_2$, and Te, calculated using the standard IMFP database[41,42] and the subshell photoionization cross sections[43,44] based on the procedure described in Refs. 45 and 46. The thickness of the activation layers are also presented in Table I, based on the intensity ratio of Ga $3d$ before and after activation following the procedure described in Ref. 32.

From Figs. 4(b) and 5(b), it is evident that, out of the total amount of Te, around 60% corresponds to Cs$_2$Te in the Cs–Te activation, and around 35% corresponds to Cs$_2$Te in the Cs–O–Te activation. The rest of the Te remains as covalent Te. Not all the Cs atoms contributed to the formation of Cs$_2$Te, a part being used in the creation of surface dipoles, namely, GaAs–Cs and GaAs–O–Cs. The Cs contributions to Cs$_2$Te, GaAs–Cs, and GaAs–O–Cs have similar binding energy positions in the Cs spectrum and cannot be resolved by XPS. The presence of the Cs contribution to the GaAs–Cs and GaAs–O–Cs dipoles is supported by the fact that there is a binding energy shift of ~0.9 eV of the Ga $3d$ and As $3d$ core levels after the activation, shifts which are commonly observed in Cs–O activation on GaAs.[27] In addition, the lack of a photoelectron peak at ~527 eV in the oxygen spectrum [Fig. 5(c)] confirms no formation of Cs$_2$O in Cs–O–Te activation.[47,48]

Two main reasons led to the record-level QE in Cs–Te and Cs–O–Te activation on GaAs. (1) The heat cleaning temperature was sufficient to desorb all the native oxides from the GaAs without degrading the surface. The GaAs surface cleanliness was verified using surface sensitive micro-spot synchrotron XPS and micro-spot LEED. One of our previous studies also showed that the high-temperature heat cleaning of GaAs in UHV does not increase the surface roughness compared with a native sample;[27] hence, it is suitable for Cs$_2$Te activation. Initial Cs depositions in both activations resulted in QE values of around 2.5% at 532 nm illumination, which also indicates the cleanliness of the GaAs surface. (2) The Cs–Te and Cs–O–Te activation procedures performed here are different from the Cs$_2$Te compound coating on GaAs created at an elevated temperature.[22] Instead of focusing on Cs$_2$Te growth at an elevated temperature, our activation was preceded by a natural course of activation at room temperature following the traditional "yo-yo" and co-deposition methods. XPS analysis showed that Cs$_2$Te indeed formed, which helped to increase the lifetime of the photocathode due to the ruggedness of the Cs$_2$Te layer to chemical poisoning and low energy ion back-bombardment. The chemical shift of both Ga $3d$
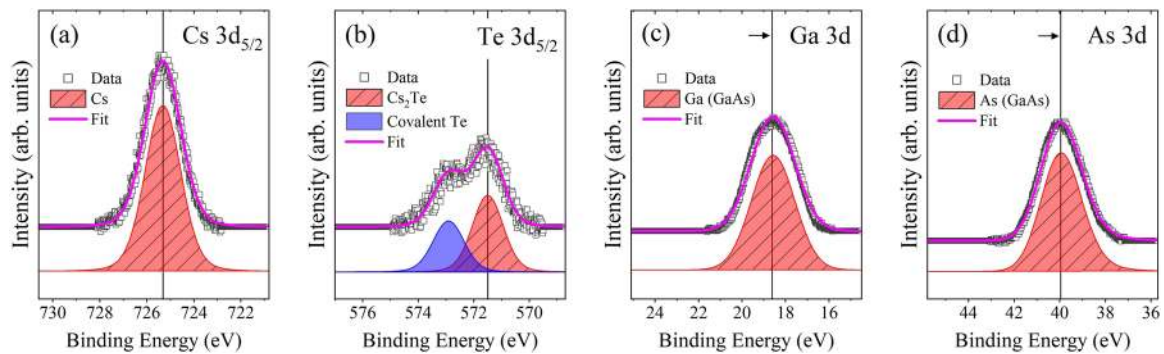
**FIG. 4**. Micro-spot synchrotron x-ray photoelectron spectra of (a) Cs $3d_{5/2}$, (b) Te $3d_{5/2}$, (c) Ga $3d$, and (d) As $3d$ core levels after the photocathode activation with Cs and Te following the procedure described in Fig. 2(a). Spectra are shown with Shirley background subtraction. Data and fit are moved upward for clarity.



**FIG. 5**. Micro-spot synchrotron x-ray photoelectron spectra of (a) Cs $3d_{5/2}$, (b) Te $3d_{5/2}$, (c) O $1s$, (d) Ga $3d$, and (e) As $3d$ core levels after the photocathode activation with Cs, $O_2$, and Te following the procedure described in Fig. 2(b). Spectra are shown with Shirley background subtraction. Data and fit are moved upward for clarity.
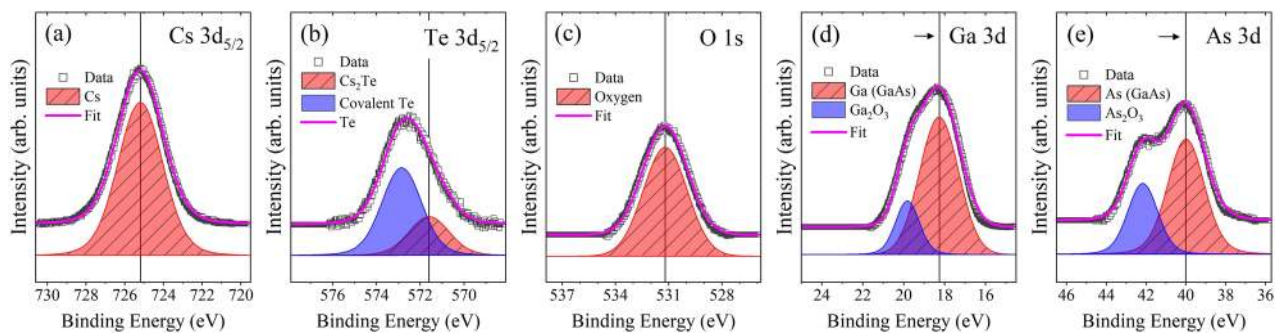
**TABLE I**. Ratio and thickness of the GaAs photocathode activated with Cs, $O_2$, and Te.

| Activation | Cs (±0.05) | Te | O (±0.05) | Thickness (±0.1 nm) |
|---|---|---|---|---|
| Cs–Te | 1.4 | 1 | . . . | 2.0 |
| Cs–O–Te | 1.2 | 1 | 1.1 | 1.2 |

and As $3d$ indicates charge transfer from Cs to GaAs, forming a surface dipole as GaAs–Cs,[11,32] which contributes to lowering the work function. In the Cs–O–Te activation process, both the GaAs–Cs and Cs–O dipoles contribute to the work function reduction. Thus, the degree of NEA is high, which leads to a high QE of around 4.5% at 780 nm illumination.

In conclusion, we have studied GaAs photocathode activation involving Cs, $O_2$, and Te. Activation with Cs–Te showed small NEA with a typical QE of around 6.6% under 532 nm laser illumination. Activation with Cs–O–Te showed significant NEA with a typical QE of around 8.8% under 532 nm laser illumination and around 4.5% under 780 nm laser illumination. The micro-spot synchrotron XPS analysis of Cs–Te and Cs–O–Te activated photocathodes showed a mixed phase of Te consisting of $Cs_2Te$ and covalent Te. Cesium also had two contributions, namely, in the formation of $Cs_2Te$

and surface dipole, such as GaAs–Cs or GaAs–O–Cs, which contributed to the NEA on GaAs.

## DATA AVAILABILITY

The data that support the findings of this study are available from the corresponding author upon reasonable request.

## REFERENCES

[1] C. K. Sinclair, Nucl. Instrum. Methods Phys. Res., Sect. A **318**, 410 (1992).
[2] R. Alley, H. Aoyagi, J. Clendenin, J. Frisch, C. Garden, E. Hoyt, R. Kirby, L. Klaisner, A. Kulikov, R. Miller, G. Mulhollan, C. Prescott, P. Sáez, D. Schultz, H. Tang, J. Turner, K. Witte, M. Woods, A. D. Yeremian, and M. Zolotorev, Nucl. Instrum. Methods Phys. Res., Sect. A **365**, 1 (1995).

[3] E. Wang, R. Lambiase, W. Liu, O. Rahman, J. Skaritka, and F. Willeke, in Proceedings of the International Particle Accelerator Conference (IPAC), Geneva, Switzerland, 2019, http://www.jacow.org.

[4] M. Kuwahara, S. Kusunoki, X. G. Jin, T. Nakanishi, Y. Takeda, K. Saitoh, T. Ujihara, H. Asano, and N. Tanaka, Appl. Phys. Lett. **101**, 033102 (2012).

[5] T. Hirose, K. Dobashi, Y. Kurihara, T. Muto, T. Omori, T. Okugi, I. Sakai, J. Urakawa, and M. Washio, Nucl. Instrum. Methods Phys. Res., Sect. A **455**, 15 (2000).

[6] D. Abbott, P. Adderley, A. Adeyemi, P. Aguilera, M. Ali, H. Areti, M. Baylac, J. Benesch, G. Bosson, B. Cade, A. Camsonne, L. S. Cardman, J. Clark, P. Cole, S. Covert, C. Cuevas, O. Dadoun, D. Dale, H. Dong, J. Dumas, E. Fanchini, T. Forest, E. Forman, A. Freyberger, E. Froidefond, S. Golge, J. Grames, P. Guèye, J. Hansknecht, P. Harrell, J. Hoskins, C. Hyde, B. Josey, R. Kazimi, Y. Kim, D. Machie, K. Mahoney, R. Mammei, M. Marton, J. McCarter, M. McCaughan, M. McHugh, D. McNulty, K. E. Mesick, T. Michaelides, R. Michaels, B. Moffit, D. Moser, C. Muñoz Camacho, J.-F. Muraz, A. Opper, M. Poelker, J.-S. Rèal, L. Richardson, S. Setiniyaz, M. Stutzman, R. Suleiman, C. Tennant, C. Tsai, D. Turner, M. Ungaro, A. Variola, E. Voutier, Y. Wang, Y. Zhang, and PEPPoCollaboration, Phys. Rev. Lett. **116**, 214801 (2016).

[7] J. J. Scheer and J. van Laar, Solid State Commun. **3**, 189 (1965).

[8] Z. Liu, Y. Sun, S. Peterson, and P. Pianetta, Appl. Phys. Lett. **92**, 241107 (2008).

[9] W. Liu and E. Wang, J. Appl. Phys. **126**, 075706 (2019).

[10] J. Zou, B. Chang, Z. Yang, Y. Zhang, and J. Qiao, J. Appl. Phys. **105**, 013714 (2009).

[11] X. Jin, A. A. C. Cotta, G. Chen, A. T. N. Diaye, A. K. Schmid, and N. Yamamoto, J. Appl. Phys. **116**, 174509 (2014).

[12] T. Maruyama, D.-A. Luh, A. Brachmann, J. E. Clendenin, E. L. Garwin, S. Harvey, J. Jiang, R. E. Kirby, C. Y. Prescott, R. Prepost et al., Appl. Phys. Lett. **85**, 2640 (2004).

[13] T. Nishitani, T. Nakanishi, M. Yamamoto, S. Okumi, F. Furuta, M. Miyamoto, M. Kuwahara, N. Yamamoto, K. Naniwa, O. Watanabe, Y. Takeda, H. Kobayakawa, Y. Takashima, H. Horinaka, T. Matsuyama, K. Togawa, T. Saka, M. Tawada, T. Omori, Y. Kurihara, M. Yoshioka, K. Kato, and T. Baba, J. Appl. Phys. **97**, 094907 (2005).

[14] W. Liu, M. Poelker, X. Peng, S. Zhang, and M. Stutzman, J. Appl. Phys. **122**, 035703 (2017).

[15] W. Liu, Y. Chen, W. Lu, A. Moy, M. Poelker, M. Stutzman, and S. Zhang, Appl. Phys. Lett. **109**, 252104 (2016).

[16] T. Siggins, C. Sinclair, C. Bohn, D. Bullard, D. Douglas, A. Grippo, J. Gubeli, G. A. Krafft, and B. Yunn, Nucl. Instrum. Methods Phys. Res., Sect. A **475**, 549 (2001).

[17] F. Machuca, Z. Liu, Y. Sun, P. Pianetta, W. E. Spicer, and R. F. W. Pease, J. Vac. Sci. Technol., B **20**, 2721 (2002).

[18] N. Chanlek, J. D. Herbert, R. M. Jones, L. B. Jones, K. J. Middleman, and B. L. Militsyn, J. Phys. D: Appl. Phys. **47**, 055110 (2014).

[19] C. K. Sinclair, in Proceedings of the 1999 Particle Accelerator Conference (Cat. No.99CH36366) (IEEE, 1999), Vol. 1, pp. 65–69.

[20] J. Grames, R. Suleiman, P. A. Adderley, J. Clark, J. Hansknecht, D. Machie, M. Poelker, and M. L. Stutzman, Phys. Rev. ST Accel. Beams **14**, 043501 (2011).

[21] W. Liu, S. Zhang, M. Stutzman, and M. Poelker, Phys. Rev. Accel. Beams **19**, 103402 (2016).

[22] J. K. Bae, L. Cultrera, P. DiGiacomo, and I. Bazarov, Appl. Phys. Lett. **112**, 154101 (2018).

[23] H. Sugiyama, K. Ogawa, J. Azuma, K. Takahashi, M. Kamada, T. Nishitani, M. Tabuchi, T. Motoki, K. Takashima, A. Era, and Y. Takeda, J. Phys.: Conf. Ser. **298**, 012014 (2011).

[24] O. Rahman, M. Gaowei, W. Liu, E. Wang, and J. Biswas, in Proceedings of the International Particle Accelerator Conference (IPAC), Geneva, Switzerland, 2019, http://www.jacow.org.

[25] J. K. Bae, A. Galdi, L. Cultrera, F. Ikponmwen, J. Maxson, and I. Bazarov, J. Appl. Phys. **127**, 124901 (2020).

[26] L. Cultrera, A. Galdi, J. K. Bae, F. Ikponmwen, J. Maxson, and I. Bazarov, Phys. Rev. Accel. Beams **23**, 023401 (2020).

[27] J. Biswas, J. Cen, M. Gaowei, O. Rahman, W. Liu, X. Tong, and E. Wang, J. Appl. Phys. **128**, 045308 (2020).

[28] S. M. Mokler, P. R. Watson, L. Ungier, and J. R. Arthur, J. Vac. Sci. Technol., B **10**, 2371 (1992).

[29] C. Deparis and J. Massies, J. Cryst. Growth **108**, 157 (1991).

[30] CasaXPS: Processing software for XPS, AES, SIMS and more.

[31] L. W. James, G. A. Antypas, J. J. Uebbing, T. O. Yep, and R. L. Bell, J. Appl. Phys. **42**, 580 (1971).

[32] C. Y. Su, W. E. Spicer, and I. Lindau, J. Appl. Phys. **54**, 1413 (1983).

[33] SAES getters.

[34] J. Jobst, L. M. Boers, C. Yin, J. Aarts, R. M. Tromp, and S. J. van der Molen, Ultramicroscopy **200**, 43 (2019).

[35] E. Bauer, Surface Microscopy with Low Energy Electrons (Springer, New York, 2014), pp. 20–25.

[36] R. U. Martinelli and D. G. Fisher, Proc. IEEE **62**, 1339 (1974).

[37] Y.-J. Zhang, J.-J. Zou, X.-H. Wang, B.-K. Chang, Y.-S. Qian, J.-J. Zhang, and P. Gao, Chin. Phys. B **20**, 048501 (2011).

[38] A. di Bona, F. Sabary, S. Valeri, P. Michelato, D. Sertore, and G. Suberlucq, J. Appl. Phys. **80**, 3024 (1996).

[39] S. Lederer, J. Han, S. Schreiber, A. Vollmer, R. Ovsyannikov, M. Sperling, H. Duerr, F. Stephan, P. Michelato, L. Monaco et al., in Proceedings of FEL 07 (JACoW, Novosibirsk, Russia, 2007), p. 457.

[40] S. Morè, S. Tanaka, S. Tanaka, Y. Fujii, and M. Kamada, Surf. Sci. **527**, 41 (2003).

[41] S. Tanuma, C. J. Powell, and D. R. Penn, Surf. Interface Anal. **21**, 165 (1994).

[42] QUASES-IMFP-TPP2M version 3.0.

[43] M. B. Trzhaskovskaya, V. I. Nefedov, and V. G. Yarzhemsky, At. Data Nucl. Data Tables **77**, 97 (2001).

[44] M. B. Trzhaskovskaya, V. I. Nefedov, and V. G. Yarzhemsky, At. Data Nucl. Data Tables **82**, 257 (2002).

[45] C. Weiland, J. Krajewski, R. Opila, V. Pallem, C. Dussarrat, and J. C. Woicik, Surf. Interface Anal. **46**, 407 (2014).

[46] S. Yasuno, S. Ishimaru, and N. Ikeno, Surf. Interface Anal. **50**, 1191 (2018).

[47] C. W. Bates, D. Das Gupta, L. Galan, and D. N. E. Buchanan, Thin Solid Films **69**, 175 (1980).

[48] C. W. Bates, T. M. van Atekum, G. K. Wertheim, D. N. E. Buchanan, and K. E. Clements, Appl. Phys. Lett. **38**, 387 (1981).